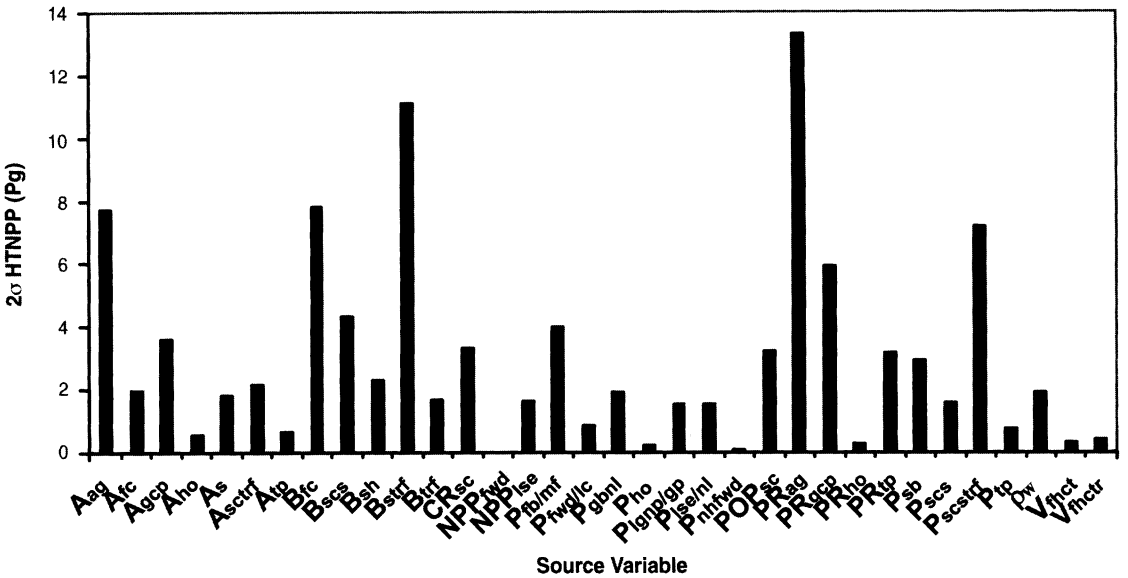

Fig. 3. Sensitivity analysis showing key independent parameters that strongly influence uncertainty in our estimate of HTNPP. Analysis was performed by systematically holding all variables (except one) constant and equal to their mean. Each parameter was allowed to vary randomly 1 million times.

$+ (POP_{sc} \times CR_{sc} \times P_{scs} \times B_{scs}) + (A_{sctrf} \times B_{trf})$

$+ (A_{fc} \times B_{fcs}) - (NPP_{fwd} \times P_{fwd/lc}) + (V_{fhct} \times \rho_w)$

$+ (V_{fhctr} \times \rho_w) + NPP_{fwd} + (A_{ho} \times P_{ho} \times PR_{ho})$

The "low calculation" of Vitousek *et al.* (*1*), because it deals only with direct consumption, by design yields an unrealistically low assessment of human impact. The "high calculation" requires speculation on the TNPP lost as a result of human activities.

10. Data in the literature usually are presented as (i) means ± standard deviations, (ii) ranges, or (iii) means. Where a choice was available, we selected the data format according to the above order. We consider global-scale studies to be those whose data are chosen to represent the country scale or larger. To reduce subjectivity, we filtered out data that would require significant manipulation (e.g., incorporating allometric rules) to be used by our model.
11. S. Brown, A. E. Lugo, *Biotropica* **14**, 161 (1982).
12. J. K. Winjum, P. E. Schroeder, *Agr. Forest Meteorol.* **84**, 153 (1997).
13. G. L. Ajtay, P. Ketner, P. Duvigneaud, in *The Global Carbon Cycle*, B. Bolin, E. T. Degens, S. Kempe, P. Ketner, Eds. (Wiley, New York, 1979), pp. 129–181.
14. R. H. Whittaker, G. E. Likens, *Hum. Ecol.* **1**, 357 (1973).
15. T. V. Armentano, C. W. Ralston, *Can. J. Forest Res.* **10**, 53 (1980).
16. S. Brown, A. E. Lugo, *Interciencia* **17**, 8 (1992).
17. Four of the parameters (P_{gbnl}, P_{ho}, $P_{lgnp/gp}$, P_{nhfwd}; see Table 1 for definitions) are difficult to estimate because of the absence of data in the literature. We used the ad hoc estimates of (*1*).
18. The ad hoc estimate of error we use, 0.50, is slightly less than the mean error for parameters with multiple data, 0.60.
19. It would be possible to derive some of the uncertainty in our estimate of HTNPP analytically, especially for aspects that involve simple summation of independent parameters. However, given that many of the parameters are multiplied and that we wished to constrain parameters to be non-negative, the Monte Carlo approach is necessary.
20. We assumed that TNPP is 120 Pg, which is a mean value derived from 30 references since 1990. For these estimates and references, see *Science* Online (www.sciencemag.org/cgi/content/full/294/5551/2549/DC1).
21. *1989 FAO Production Yearbook* (FAO, Rome, 1990).
22. C. Brown, *Working Paper No. GFPOS/WP/03* (FAO, Rome, 1999).
23. D. Pandey, *Report to Food and Agriculture Organisation of the United Nations Project GCP/INT/628/UK* (FAO, Rome, 1997).
24. D. Pandey, *FAO Forestry Paper 128* (FAO, Rome, 1995).
25. *The Forest Resources of the Tropical Zone by Main Ecological Regions* (FAO, Rome, 1992).
26. G. Bull, W. Mabee, R. Scharpenberg, *Global Fibre Supply Model* (FAO, Rome, 1998).
27. *FAO Forestry Paper 124* (FAO, Rome, 1995).
28. Our estimates of uncertainty are conservative in that (i) estimates of parameters are not independent (i.e., they are influenced by older literature, and some newer estimates are reworkings of older ones), and (ii) uncertainty due to assumptions in the model used (template, Fig. 1) is not included.
29. A well-known study (*31*) used frequently by others has a typographical error (H. Lieth, personal communication) in its estimate of productivity of cultivated land, and we filtered out its estimates in our analysis.
30. C. S. Potter *et al.*, *Global Biogeochem. Cycles* **7**, 811 (1993).
31. H. Lieth, *Hum. Ecol.* **1**, 303 (1973).

32. Supported in part by a grant from the NASA Land-Surface Hydrology Program. We thank R. Oren and W. Schlesinger for helpful reviews of this manuscript.

13 July 2001; accepted 8 November 2001

A DNA Microarray-Based Genetic Screen for Nonhomologous End-Joining Mutants in *Saccharomyces cerevisiae*

Siew Loon Ooi,[1] Daniel D. Shoemaker,[2] Jef D. Boeke[1]*

We describe a microarray-based screen performed by imposing different genetic selections on thousands of yeast mutants in parallel, representing most genes in the yeast genome. The presence or absence of mutants was detected by oligonucleotide arrays that hybridize to 20-nucleotide "barcodes." We used this method to screen for components of the nonhomologous end-joining (NHEJ) pathway. Known components of the pathway were identified, as well as a gene not previously known to be involved in NHEJ, *NEJ1*. Nej1 protein interacts with the amino terminus of LIF1/XRCC4, a recently recognized "guardian of the genome" against cancer.

A worldwide effort to create a comprehensive genetic resource has resulted in a nearly complete collection of deletion alleles corresponding to the yeast open reading frames (ORFs) (*1*, *2*). Over 5800 of the estimated 6000-plus yeast ORFs have been systematically disrupted. In each mutant the ORF is precisely replaced by a *kanMX* cassette that confers G418 resistance. In addition, each cassette contains two 20-nucleotide (nt) "barcodes" uniquely assigned to that gene. The sequences, called UPTAGs and DOWNTAGs, are flanked by universal priming sites and can be used as

[1]Department of Molecular Biology and Genetics, Johns Hopkins University School of Medicine, 617 Hunterian Building, 725 North Wolfe Street, Baltimore, MD 21205, USA. [2]Rosetta Inpharmatics Inc., 12040 115th Street Avenue Northeast, Kirkland, WA 98034, USA.

*To whom correspondence should be addressed. E-mail: jboeke@jhmi.edu

hybridization probes for the presence of each mutant (Web fig. 1; supplementary Web material is available on *Science* Online at www.sciencemag.org/cgi/content/full/1065672/DC1) (*3*). The resultant hybridization patterns can be used to determine the presence, absence, or under- or overrepresentation of a particular mutant in the population (*1*, *2*, *4*).

We applied this technique to the study of the nonhomologous end-joining (NHEJ) pathway, a eukaryotic cellular pathway critical to double-strand break repair, antigen-receptor gene rearrangement, neurogenesis, radiation resistance, and cancer (*5*, *6*). Most genes involved in NHEJ are conserved from *Saccharomyces cerevisiae* to mammals. To date, the proteins known to affect NHEJ in *S. cerevisiae* are Yku70p and Yku80p, Lig4p, Lif1p, Rad50p, Mre11p, Xrs2p, Sir2p, Sir3p, and Sir4p (Web fig. 2) (*7*–*9*). The Yku70p/Yku80p heterodimer has DNA end-binding activity and functions in the early step of end joining. In vitro, the Rad50p/Mre11p complex has single-stranded DNA (ssDNA) endonuclease and double-stranded DNA (dsDNA) 3′→5′-exonuclease activities. Xrs2p probably links the Rad50p/Mre11p complex to damage-induced cell cycle checkpoints. The final step in the NHEJ pathway, joining of the DNA ends, is catalyzed by DNA ligase IV (Lig4p) together with its associated protein Lif1p. The mammalian homologs of Lig4p and Lif1p, DNA ligase IV and XRCC4, are implicated in V(D)J recombination, neural apoptosis, and radiation resistance (*5*, *6*).

We used a transformation-based plasmid repair assay (*10*) to screen for NHEJ-defective mutants. NHEJ is required for efficient transformation of plasmids linearized at sites lacking sequence homology to the yeast genome. Mutants defective in NHEJ are recovered very inefficiently when transformed with linearized plasmids, but they are transformed efficiently with circular plasmids.

Pools of mutant cells were made by combining 5-mm circular patches of each mutant grown on YPD plates at 30°C for 3 days (*11*). Both a *MAT***a** haploid deletion pool and a *MAT***a**/*MAT*α diploid deletion pool in which each mutant allele was homozygous were constructed and assayed separately. The haploid pool was analyzed because it contained more mutants. Diploids were assayed because in principle, the genetic "quality" of the diploid deletion strains is higher; diploids were made by mating two independently derived haploid mutants. Therefore, using diploid mutants lessens the possibility that an observed phenotype results from a collateral mutation unrelated to the original tagged mutation. Finally, NHEJ is a cell type–regulated process, because mating-competent cells perform NHEJ more efficiently than mating-incompetent cells regardless of ploidy (*8*, *9*). It is therefore interesting to compare each mutant's end-joining activity in both mating-competent haploid and mating-incompetent diploid cells. Naturally, because all mutants in the pools are null alleles, this strategy only permits the identification of nonessential genes. The haploid and homozygous diploid deletion pools contained 4647 and 3546 different mutations, respectively.

Pools of mutants were made competent and transformed (*12*) with circular centromeric pRS416 and Eco RI–linearized pRS416 plasmid in parallel. The transfor-

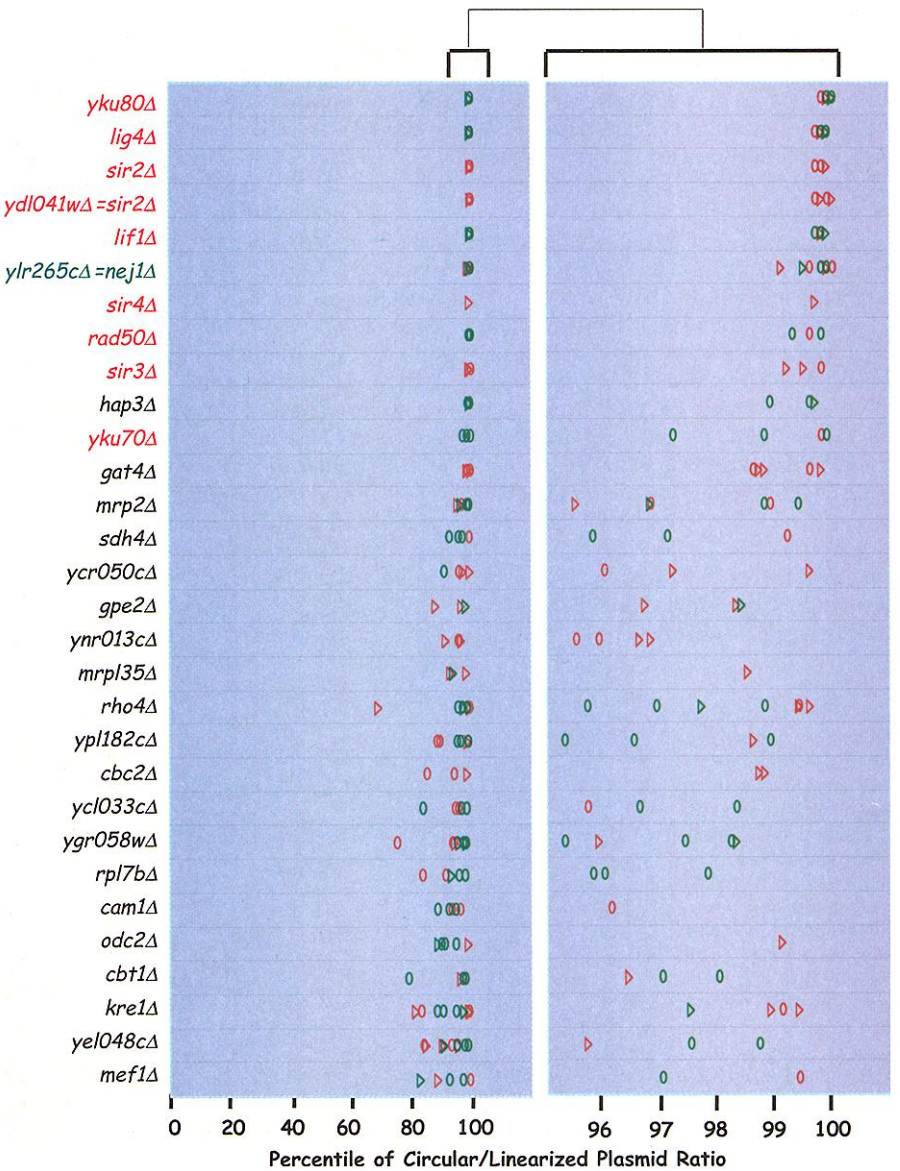

Fig. 1. Deletion strains with the most severe NHEJ defect. Five and four microarray hybridizations were performed on haploid (two DOWNTAGs and three UPTAGs) and diploid (three DOWNTAGs and one UPTAG) transformations, respectively. For each microarray experiment, the circular/linearized transformation ratio obtained for each tag was used to rank the tags. The rank of each tag was then used to derive the percentile of each tag. The percentile is used so that ratios obtained for each tag from the nine separate hybridization analyses could be compared with each other. For each tag, the average percentile of the nine microarray hybridizations was calculated and used to sort the deletion strains. The 30 deletion strains with the highest average percentiles are shown in decreasing order. Only deletion strains analyzed in four or more microarray experiments were plotted, with the exception of *sir4*Δ, which is known to affect NHEJ but has only a single data point. Color denotes data points obtained from either haploid (red) or diploid (green) mutant pools. The symbols denote data points obtained from either DOWNTAG (circle, ○) or UPTAG (triangle, △) microarray analyses. Mutants known to have NHEJ defects are colored red. *nej1*Δ is the new NHEJ-defective mutant found in this screen.

mants were spread at a density of 10^4 to 10^5 colonies per plate on 10 150-mm petri plates containing SC-Ura medium. Previous control experiments indicated that when the total number of transformants analyzed dropped below 10^5 colonies, the loss of signal from poorly represented pool members resulted in decreased reproducibility of hybridization. DNA was prepared from the pooled transformants (*13*) and probes were prepared by polymerase chain reaction (PCR) with Cy3- and Cy5-labeled primers (see the legend of Web fig. 3). Cy3 and Cy5 were used to label the probes for the linear and circular plasmid transformations, respectively. The labeled probes were then hybridized to oligonucleotide arrays containing either all UPTAG or all DOWNTAG barcodes and scanned (see the legend to Web fig. 3). Each barcode was represented in triplicate on an array.

Two independent parallel transformations were carried out for both haploid and diploid deletion pools (Web table 1). We performed nine microarray analyses in total, five in haploids (two DOWNTAGs and three UPTAGs) and four in diploids (three DOWNTAGs and one UPTAGs). The mutants known to be defective in NHEJ showed consistent hybridization defects in the samples transformed with linear DNA, as expected (Web fig. 3A). Scatterplots indicated good reproducibility between different transformation experiments. Normalized signal mean from samples subjected to the same condition but from independent transformations correlated at $r = 0.80$ or better (Web fig. 3B). Transformation ratios were derived by dividing the normalized signal mean of circular plasmid by that of linear plasmid for each mutant, respectively. Thus, mutants with high ratios are defective in NHEJ.

To evaluate the multiple data sets generated in haploid and diploid pools, we plotted the percentile rank of the circular/linearized transformation ratio for each mutant (see the legend to Web fig. 3). The 30 deletion strains with the highest average percentile are shown in decreasing order (Fig. 1). Consistently high percentiles were observed for the known NHEJ mutants in multiple hybridization experiments. Ratio data were not obtained for *mre11*Δ and *xrs2*Δ because their hybridization signals in both the control and experimental conditions did not satisfy the signal-to-noise ratio criterion used (see the legend to Web fig. 3). Certain mutants were previously reported to have a three- to fivefold decrease in NHEJ in the plasmid repair assay (*14*, *15*). Four of seven such mutants were assayed in our microarray analysis. However, these haploid mutants did not show high average (mean ± SD) percentiles: *rad9*Δ (81 ± 17%), *rad17*Δ (37 ± 31%), *rad24*Δ (15 ± 12%), *srs2*Δ (34 ± 30%). Our failure to observe NHEJ defects in these mutants may reflect differences in the strain background used. In contrast, mutations in the 10 NHEJ genes described earlier typically have 50- to 100-fold decreases in NHEJ efficiency in the plasmid repair assay in haploid yeast cells. Previous studies suggest that although DNA-dependent protein kinase (DNA-PK) is essential for NHEJ in mammalian cells, its homolog, Tel1p, is not required in yeast (*16*). Similarly, IP6 was found to bind DNA-PK and stimulate mammalian NHEJ activity in vitro (*17*); we do not see any evidence that *IPK1*, one of the kinases required for IP6 synthesis, affects NHEJ in our experiments. About 13% (600 of 4647 mutants) of the haploid and 14% (500 of 3546 mutants) of the homozygous diploid mutants did not satisfy the signal-to-noise ratio criterion used, and thus no data were obtained for these mutants. These mutants probably have growth or transformation defects.

One mutant not previously known to have a defect in NHEJ, *nej1*, also showed high average (mean ± SD) percentile: 99.7 ± 0.3% (Fig. 1). *nej1* was retested individually to confirm that it had reduced transformation efficiency with linearized plasmid. The *nej1* mutant was as defective in linear plasmid transformation as the *yku80* and *lig4* mutants (Fig. 2A). A complementation test was performed by evaluating *nej1* strains containing an empty

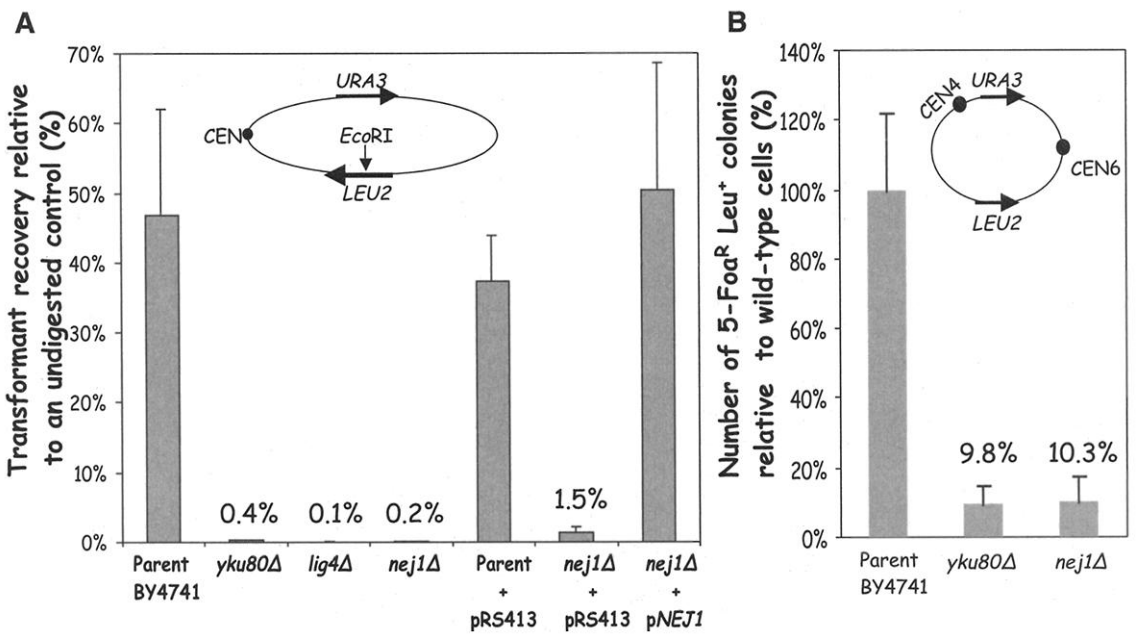

Fig. 2. The *nej1* mutant is defective in nonhomologous end joining. (**A**) A *MAT***a** haploid strain of the *nej1* mutant and control strains were subjected to individual plasmid repair assays with pSO98 (cartoon). pSO98 is a pRS416-based CEN plasmid containing both *URA3* and *LEU2*. The indicated deletion strains were transformed with 0.4 μg of supercoiled or Eco RI–linearized pSO98 and plated onto SC-Ura plates. For the complementation test, each plasmid-containing strain was transformed with the same plasmid under identical conditions. However, the transformants were plated onto SC-Leu-His plates to prevent transformants generated by homologous recombination between the two plasmids. The value plotted is the number of transformants obtained from linearized plasmid expressed as a percentage of the transformants obtained from supercoiled plasmid. *PNEJ1* was constructed by PCR-amplifying the *NEJ1* fragment extending from 307 base pairs (bp) upstream and 418 bp downstream flanking the *NEJ1* coding sequence and inserting it into pRS413. The end-joining defect of the *nej1* mutant was complemented by p*NEJ1*. Data represent the mean ± SD of three independent transformations. (**B**) Dicentric plasmid repair assay. To assay for repair of a dicentric plasmid, each deletion strain was transformed with pSO99 (cartoon) and plated onto SC-Ura-Leu plates. pSO99 is a CEN6 and CEN4 dicentric plasmid carrying both *LEU2* and *URA3* fragments. CEN4 and *URA3* fragments are adjacent to each other. For each strain, 5×10^7 and 1×10^7 transformed cells were plated onto SC-Leu plates with or without 5-fluoro-orotic acid (5-FOA). The number of 5-FOA–resistant Leu^+ colonies for each strain was normalized to that of the wild-type strain and plotted. Data represent the mean ± SD of three independent experiments.

vector or a cloned *NEJ1* gene. Full complementation of the *nej1* mutant defect was observed, indicating that the observed defect was in fact due to the *nej1* deletion. We also tested whether *nej1* strains were defective in an independent assay for NHEJ—the dicentric plasmid rearrangement test, which assays for the frequency of rejoining of broken DNA ends generated by dicentric plasmids pulled to opposite poles during mitosis. In contrast to the plasmid repair assay, the DNA substrates in this test are heterogeneous with regard to end structure, allowing us to probe the *nej1* mutant's end-joining activity on a broader range of substrate types (*18*). The *nej1* and *yku80* mutants had similar defects in NHEJ in this assay (Fig. 2B).

The *nej1* mutant is defective in two different assays for NHEJ. However, it is not clear whether Nej1p has a direct or indirect role in NHEJ. The amino acid sequence of Nej1p is not phylogenetically conserved. However, several additional pieces of evidence suggest that Nej1p plays a critical role in the metabolism of dsDNA breaks in vivo. When compared with NHEJ mutants blocked at various steps of the pathway, the phenotypes of the *nej1* mutant are most similar to those of *lif1* and *lig4* mutants. This conclusion is based on the lack of a mating defect in *nej1*, its relatively normal telomere length (Web fig. 4A), and its normal ability to perform homologous recombination.

Moreover, in a high-throughput two-hybrid assay analysis, Nej1p was found to interact with Lif1p (*19*), an essential component of DNA ligase IV, the specialized ligase used in the NHEJ pathway (*20*). We confirmed the Nej1p-Lif1p protein-protein interaction and mapped the interaction domains in Nej1p and Lif1p. Residues 150 to 342 of Nej1p suffice for interaction with Lif1p, whereas residues 2 to 200 of Lif1p suffice for interaction with Nej1p (Fig. 3A). The Nej1p-interacting domain of Lif1p is distinct from its Lig4p interaction domain (Fig. 3A) (*19*). On the basis of additional two-hybrid assays, Nej1p is not required for the Lif1p-Lig4p interaction, nor is Lig4p required for the Lif1p-Nej1p interaction (Web fig. 4B). Interestingly, Nej1p interacts with the NH_2-terminal domain of Lif1p, and recent structural work on human Lif1 homolog, XRCC4, revealed that this NH_2-terminal globular domain may also interact with DNA (*21*) (Fig. 3B). These results suggest the formation of a possible ternary Lif1p-Lig4p-Nej1p complex during NHEJ, and that Nej1p acts together with Lig4p and Lif1p in an essential late step in the NHEJ pathway (Fig. 3B). Since we began this work, other groups have discovered *NEJ1*'s role in

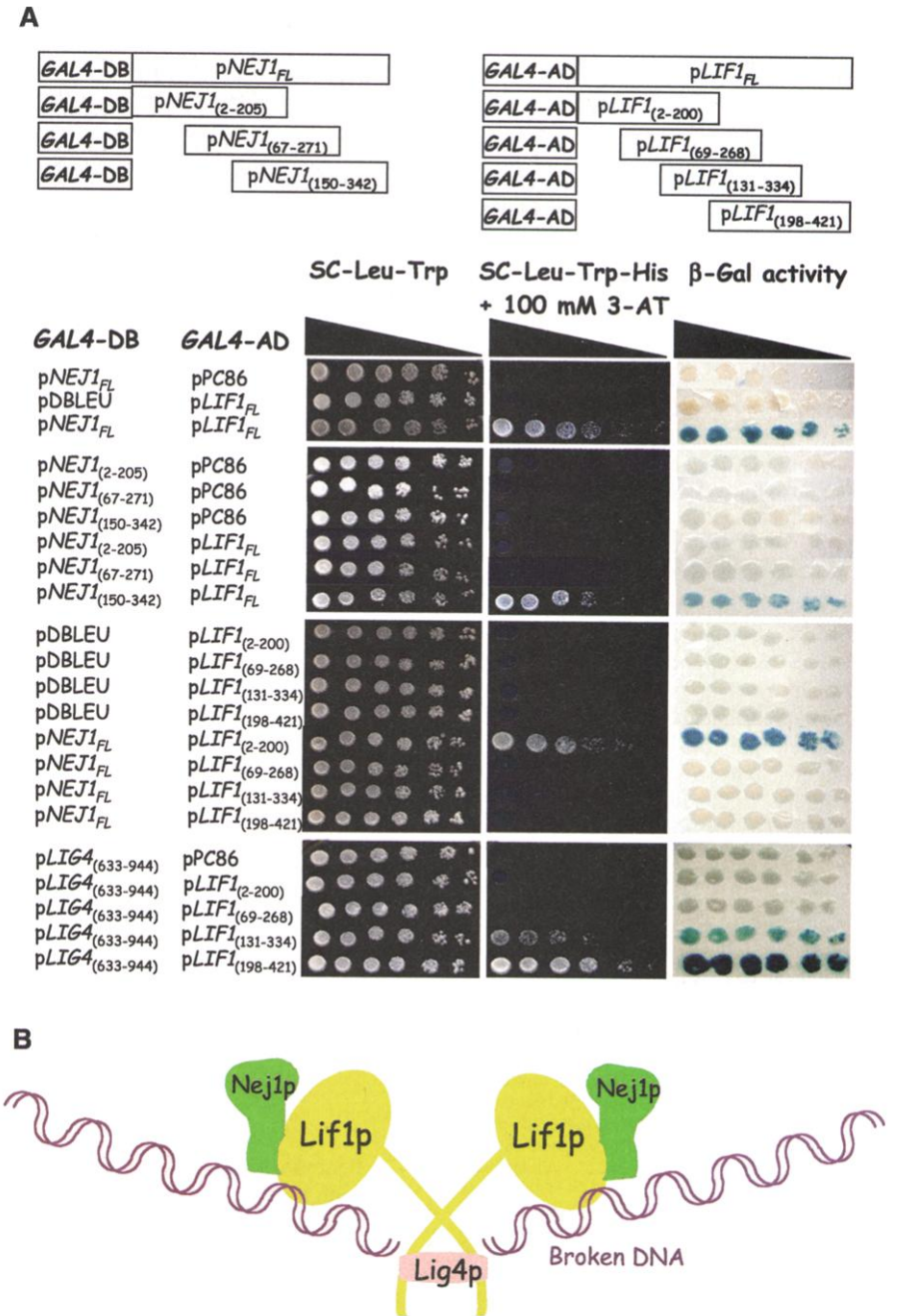

Fig. 3. (**A**) Nej1p interacts with Lif1p. pDBLEU and pPC86 are the parental plasmids encoding the *GAL4* DNA-binding and DNA-activation domains, respectively. DNA fragments representing full-length codons 2 to 205, 67 to 271, and 150 to 342 of the *NEJ1* ORF and codons 633 to 944 of the *LIG4* ORF were fused to the *GAL4* DNA-binding domain in pDBLEU. DNA fragments representing full-length codons 2 to 200, 69 to 268, 131 to 334, and 198 to 421 of the *LIF1* ORF were fused to the GAL4 DNA-activation domain in pPC86. Two-hybrid interaction was tested with the MaV203 strain, which bears *HIS3*, *URA3*, and *lacZ* reporters (*26*). The cell density of each transformant was adjusted to 1 OD/ml, and fivefold serial dilutions were prepared and spotted onto control (SC-Leu-Trp) and experimental (SC-Leu-Trp-His + 100 mM 3-AT) plates to test for protein interaction. Cells were incubated at 30°C for 2 days. β-Galactosidase assays were performed as described (*26*). The subscript specifies the amino acid codons expressed in the fusion plasmid. FL denotes the full-length protein. (**B**) Model for interaction of Lig4p, Lif1p, Nej1p, and broken DNA. On the basis of the two-hybrid data and the structural data of Junop *et al.* (*21*), we proposed that the COOH-terminus of Nej1p interacts with the NH_2-terminal globular domain of Lif1p. This domain has a mostly acidic surface, except for a single basic surface proposed to bind DNA (*21*). Because the COOH-terminus of Nej1p is rich in basic residues, it probably interacts with the acidic surface of Lif1p. The basic residues in the Nej1p could also stabilize the Lif1p:DNA interaction through direct DNA contacts. Lig4p interacts with the Lif1p COOH-terminal domain, which is a long α helix involved in dimer and higher order multimer formations. These dimers are proposed to stabilize broken DNA ends and ultimately allow their joining.

NHEJ, using screens for genes up-regulated in haploids versus diploids (*22, 23*) or using two hybrid-screens with Lif1p (*24*).

hap3 mutants also showed a high average (mean ± SD) percentile (99.3 ± 0.4%) in diploid microarray analyses (Fig. 1). Preliminary results suggest that diploid *hap3* mutants have modest linear-plasmid transformation defects. However, when diploid *hap3* mutants were transformed with Eco RI–digested pSO98 (see the legend to Fig. 2A) and plated onto SC-Leu to select for precisely rejoined transformants, diploid *hap3* mutant transformation efficiency was not distinguishable from that of wild-type cells, whereas *yku80* mutants had a fivefold-reduced transformation efficiency.

We have shown here that pools of thousands of mutants generated by DNA transformation can be analyzed in parallel. This approach is likely to have many important applications in any genetic screen requiring a plasmid. Furthermore, this approach makes feasible genetic screens for quantitative phenotypes such as NHEJ frequency, mutation rate, and gross chromosomal rearrangement rate, which are physically too labor-intensive to be carried out by conventional screening methods. Finally, databases containing quantitative phenotypic information of this type will provide an important resource for mapping genetic-interaction networks.

References and Notes

1. E. A. Winzeler *et al.*, *Science* **285**, 901 (1999).
2. D. D. Shoemaker, D. A. Lashkari, D. Morris, M. Mittman, R. W. Davis, *Nature Genet.* **14**, 450 (1996).
3. The UPTAG and DOWNTAG features allow large numbers of deletion strains to be pooled and analyzed in parallel. The pool of mutants was transformed with either circular or Eco RI–linearized pRS416 and plated onto SC-Ura plates. Genomic DNA was isolated from pooled Ura$^+$ transformants and used as a PCR template to amplify the DOWNTAGs or UPTAGs of the strains present. Genomic DNA from the circular pRS416-transformed cells was amplified with Cy5 (red)-labeled universal primer, whereas that of the Eco RI–linearized pRS416-transformed cells was amplified with Cy3 (green)-labeled universal primers. These fluorescently labeled probes were then cohybridized to a DNA microarray bearing each tag in triplicate. An NHEJ-defective deletion strain would be underrepresented in the Eco RI–linearized plasmid-transformed pool and would have a reduced signal in the Cy3 channel (Web fig. 1B).
4. G. Giaever *et al.*, *Nature Genet.* **21**, 278 (1999).
5. D. C. van Gent, J. H. Hoeijmakers, R. Kanaar, *Nature Rev. Genet.* **2**, 196 (2001).
6. D. B. Roth, M. Gellert, *Nature* **404**, 823 (2000).
7. L. K. Lewis, M. A. Resnick, *Mutat. Res.* **451**, 71 (2000).
8. S. U. Åstrom, S. M. Okamura, J. Rine, *Nature* **397**, 310 (1999).
9. S. E. Lee, F. Paques, J. Sylvan, J. E. Haber, *Curr. Biol.* **9**, 767 (1999).
10. S. J. Boulton, S. P. Jackson, *Nucleic Acids Res.* **24**, 4639 (1996).
11. Construction of the deletion strain pools: To construct the deletion pools, collections of 4647 *MAT***a** haploid mutants (Research Genetics) or 3546 homozygous diploid mutants (gift of M. Johnston) were pinned as individual 5-mm patches onto YPD plates containing G418 (200 μg/ml) and incubated at 30°C for 3 days. The mutants were scraped into ~300 ml of 15% glycerol. The optical densities at 600 nm (OD_{600}) of the deletion pools were adjusted to 15 OD_{600}/ml with 15% glycerol, and pools were frozen in 1- to 2-ml samples.
12. Competent cell preparation: 2 ml of 15 OD_{600}/ml frozen mutant pool were added to ~300 ml of YPD to obtain an initial starting OD of 0.125 OD_{600}/ml. The culture was then shaken at 30°C for ~5 hours to an OD of 0.5 OD_{600}/ml. The culture was harvested, and then washed once in water and once in 0.1 M LiOAc. The cells were then adjusted to 0.2 OD_{600}/μl in about 800 μl of 0.1 M LiOAc. Yeast transformation: For each transformation, 150 μl of competent cells were used. The number of colonies required for reproducible hybridization results was 10^5 to 10^6. Circular pRS416 and Eco RI–digested pRS416 were used to transform each deletion pool (Web table 1). Ten microliters of sheared, heat-denatured herring sperm DNA (10 mg/ml) was added to the transforming DNA, followed by the addition of 150 μl of competent cells and 444 μl of 45.4% polyethylene glycol (PEG-3350) in 0.1 M LiOAc. Cells were rotated in a 30°C incubator for 30 min. Dimethyl sulfoxide (67 μl) was then added and cells were heat-shocked at 42°C for 15 min. Cells were washed and resuspended in 4.2 ml of water. The transformation reaction was then plated onto 10 150-mm SC-Ura plates and incubated at 30°C for 2 to 3 days.
13. Genomic DNA preparation: The cell suspensions from 10 plates (~30 ml) were pooled and then mixed thoroughly by vortexing, and 10 to 15 OD units of cell pellet was used for genomic DNA preparation. The rest of the pellet was resuspended in 15% glycerol and stored at −70°C. Genomic DNA was prepared as described (*25*), followed by ribonuclease A digestion, phenol chloroform extraction, and ethanol precipitation.
14. V. Hegde, H. Klein, *Nucleic Acids Res.* **28**, 2779 (2000).
15. M. de la Torre-Ruiz, N. F. Lowndes, *FEBS Lett.* **467**, 311 (2000).
16. S. J. Boulton, S. P. Jackson, *EMBO J.* **17**, 1819 (1998).
17. L. A. Hanakahi, M. Bartlet-Jones, C. Chappell, D. Pappin, S. C. West, *Cell* **102**, 721 (2000).
18. Y. Tsukamoto, J. Kato, H. Ikeda, *Mol. Gen. Genet.* **255**, 543 (1997).
19. G. Herrmann, T. Lindahl, P. Schar, *EMBO J.* **17**, 4188 (1998).
20. T. Ito *et al.*, *Proc. Natl. Acad. Sci. U.S.A.* **98**, 4569 (2001).
21. M. S. Junop *et al.*, *EMBO J.* **19**, 5962 (2000).
22. A. Kegel, J. O. Sjostrand, S. U. Astrom, *Curr. Biol.* **11**, 1611 (2001).
23. M. Valencia *et al.*, *Nature*, in press.
24. M. Frank-Vaillant, S. Marcand, *Genes Dev.* **15**, 3005 (2001).
25. J. D. Boeke, D. J. Garfinkel, C. A. Styles, G. R. Fink, *Cell* **40**, 491 (1985).
26. M. Vidal, R. K. Brachmann, A. Fattaey, E. Harlow, J. D. Boeke, *Proc. Natl. Acad. Sci. US.A.* **93**, 10315 (1996).

27. We thank all members of the *Saccharomyces* Genome deletion project consortium [see (*1*)] for the collection of deletion mutants. We thank I. Celic and A. IJpma for encouragement and technical assistance; T. Gunatilaka and D. Zack for help with scanning; N. Bachman, C. Connelly, M. Lee, and S. Sookhai-Mahadeo for help with deletion pools; and M. Johnston and E. Winzeler for strains and helpful discussions. E. Bolton, B. Cormack, D. Koshland, J. Pevsner, F. Spencer, and D. Yuan provided helpful discussions and J. Haber, S. Åstrom, M. Frank-Vaillant, and S. Marcand provided discussions and shared unpublished results. Supported by NIH grants HG01627 and GM36481.

23 August 2001; accepted 17 October 2001
Published online 8 November 2001;
10.1126/science.1065672
Include this information when citing this paper.

Role of the Hrp Pilus in Type III Protein Secretion in *Pseudomonas syringae*

Qiaoling Jin and Sheng-Yang He*

Bacterial surface appendages called pili and needle-like filaments are associated with protein and/or DNA transfer to recipient plant, human, or bacterial cells during pathogenesis or conjugation. Although it has long been suspected that pili function as a conduit for protein or DNA transfer, direct evidence has been lacking. The Hrp pilus of *Pseudomonas syringae* is assembled by the type III secretion system. We used an in situ immunogold labeling procedure to visualize the extrusion of an effector protein, AvrPto, from the tip of the Hrp pilus, providing direct evidence that a bacterial pilus can function as a conduit for protein delivery.

Pili are nonflagellate filamentous surface appendages produced by virtually every species of Gram-negative bacterium. Pili are known to function as a means of attaching bacteria to various surfaces, often playing a crucial role in bacterial infection of humans and plants. Several pili are also required for delivery of effector proteins and DNA into recipient host or bacterial cells (*1–4*). Although the long and thin pili appear to be especially suited for long-distance protein and DNA delivery, direct evidence showing the extrusion of effector proteins or DNA from the tip of a pilus has never been shown.

The Hrp pilus of *Pseudomonas syringae* pv. *tomato* strain DC3000 (hereafter *Pst* DC3000) is assembled by the *hrp* gene–encoded type III secretion system (*4–8*). This pilus is composed of a major subunit, the HrpA protein. The *hrpA* gene is required directly or indirectly for the secre-

Department of Energy Plant Research Laboratory and Department of Plant Biology, Michigan State University, East Lansing, MI 48824, USA.

*To whom correspondence should be addressed. E-mail: hes@msu.edu